

Transport Phenomena during Liquid Si-Induced 4H-SiC Surface Structuring in a Sandwich Configuration

JOUSSEAUME Yann^{1,a}, CAUWET François^{1,b}, FERRO Gabriel^{1,c}

¹Laboratoire des Multimatériaux et Interfaces, UMR CNRS 5615, 6 rue Victor Grignard, Lyon 1 University, 69622 Villeurbanne (France)

^ayann.jousseume@univ-lyon1.fr, ^bfrancois.cauwet@univ-lyon1.fr, ^cgabriel.ferro@univ-lyon1.fr

Keywords: 4H-SiC, Surface structuration, Morphology, Liquid silicon, Carbon transport

Abstract. 4H-SiC/Si_(liq)/4H-SiC stacks were treated at 1550-1600°C under H₂ in a RF-heated cold-wall reactor in order to generate macrosteps-structuring of the 4°off SiC(0001) wafers. Using 400 µm thick liquid Si, the observed important matter transport from the edges to the center of the same wafer was attributed to RF-induced convection rolls inside the thick liquid Si. When the liquid thickness was reduced down to 30 µm, the matter transport followed this time the vertical thermal gradient like in the case of liquid phase epitaxy. The dissolution rate of the bottom (hotter) wafer was found to increase from 1.7 µm/h at 1550°C to 3.3 µm/h at 1600°C. The use of H₂ gas was found essential to the system since it does not generate gas trapping (unlike Ar) and it participates to the creation of the vertical thermal gradient.

Introduction

Despite the attractive properties and already wide use of 4H-SiC for power electronics, the performances of SiC MOSFETs remain limited due to low channel mobility. This is mainly attributed to electrically active defects at the SiO₂/SiC. While the origin of these interface defect states (D_{it}) is still under debate, experimental studies attribute them to the micro-stepped morphology of the 4°off epitaxial surfaces used [1]. Such morphology is expected to directly impact the creation of the SiO₂/SiC interface by eventually initiating non-ideal oxidations and nonstoichiometric near-interface regions [2]. Previous studies have shown that a MOS capacitor fabricated on macrostepped surfaces shows a systematic decrease of D_{it} of ~10-15% compared to “standard” samples [3]. A simple way for fabricating such 4H-SiC macrostepped surface is to put it in contact with a liquid Si. Toward this end, we recently explored a sandwich configuration where a bulk piece of silicon is melted between two 4H-SiC (0001) 4°off Si-face wafers [4]. It was successful for spreading uniformly the liquid Si and forming highly step-bunched surfaces. However, homogeneity and step regularity were not easy to reach, because of some complex transport phenomena inside the liquid Si. The goal of the present work is to study and identify these transport phenomena in order to optimize the process.

Experimental

The SiC/Si/SiC sandwich configuration used is schematized in Fig. 1. It consists in a piece of n type Si wafer placed in between two 4H-SiC (0001) 4°off Si-face wafers from SK Siltron (see Fig. 1). With this setup, both Si faces of the top and bottom 4H-SiC wafers are in contact with the molten Si. The lateral size of the bottom SiC wafer is larger than the top one, i.e. 2x2 and 1.2x1.2 cm² respectively to avoid any Si loss upon melting from the 4H-SiC wafers sides. Such configuration leads to natural spreading of the liquid Si and homogeneous thickness of this liquid. We will thus assume that the area occupied by the liquid Si is equal to the surface of the SiC-top wafer, with no liquid overflow (as confirmed experimentally). Each Si piece is weighed before experiment so that, from this mass m_{Si} and the area S occupied upon melting, one can calculate the Si thickness th_{Si} between the two SiC pieces using the following equation:

$$th_{Si(\mu m)} = \frac{m_{Si(g)}}{d_{Si} \times S} \times 10^4$$

with d_{Si} the Si density (in g.cm^{-3}), and S the area of the top-SiC wafer (1.44 cm^2). In this work, two different thicknesses of the Si liquid phase were compared: $30 \text{ }\mu\text{m}$ and $400 \text{ }\mu\text{m}$.

After ultrasonic cleaning in methanol of each part of the assembly, the stacking is placed upon a graphite susceptor which is then inserted in a RF-heated homemade vertical cold wall. The experiments were performed under 12 slm of H_2 and not under Ar for the following reasons: 1) it avoids the formation of gas trapping (which is often observed with the use of Ar [5]) and 2) the high thermal conductivity of H_2 can generate a substantial vertical thermal gradient inside the stacking which is a very important factor in this reconstruction process (this aspect will be more detailed in another paper of the same authors to be presented at ICSCRM2022). The structuring experiments were performed at $1550\text{--}1600^\circ\text{C}$ for 15–180 min. After the thermal treatments, the samples were wet etched in HF/HNO_3 for removing the Si and thus separating both wafers. After surface morphology observation by various means, surface mapping was obtained by mechanical profilometry in order to estimate the long-range homogeneity of the surface structuring process and to visualize and quantify any possibly occurring mass transport phenomenon inside the assembly.

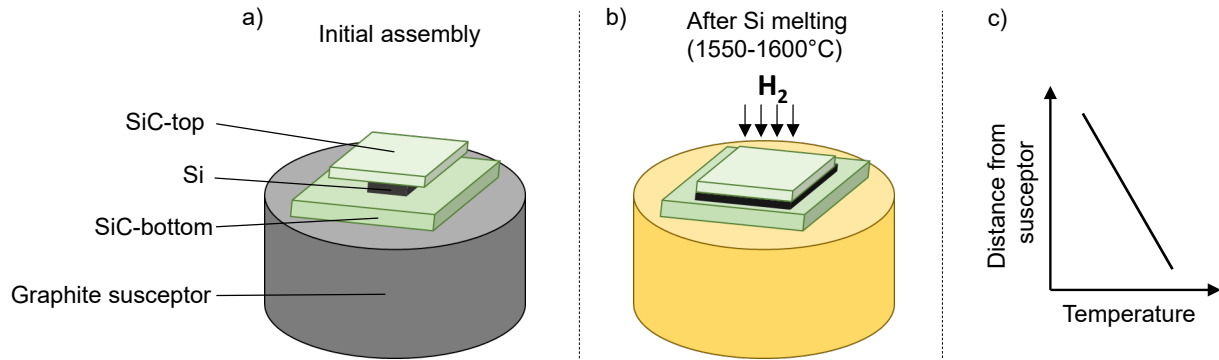


Figure 1. Schematic drawings of the investigated sandwich setup: a) before and b) after Si melting; c) the presumed vertical thermal gradient inside the assembly using this configuration.

Results and Discussion

Fig. 2 shows the obtained surface mapping and the corresponding surface morphology for samples treated at 1550°C with 30 and $400 \text{ }\mu\text{m}$ Si thickness. First of all, as expected, all the wafers in contact with liquid Si were macro-stepped reconstructed with step width in the $1\text{--}5 \text{ }\mu\text{m}$ range. Apart from this reconstruction, the use of $30 \text{ }\mu\text{m}$ thick Si liquid phase obviously leads to flatter surfaces than with $400 \text{ }\mu\text{m}$, for both top and bottom wafers. In the latter case, a butterfly-like pattern can be observed with positive height (up to $+6 \text{ }\mu\text{m}$) in the center while the peripheries are delimited with deep depressions (from -6 to $-8 \text{ }\mu\text{m}$). The butterfly-like pattern should result from material gain and thus epitaxial SiC deposition. Conversely, the edge depressions should correspond to material loss and thus SiC etching. By combining these two observations, one could propose that some SiC matter transport may occur from the edges to the center. Note that if growth occurs at the center of the bottom (hotter) wafer, it should be against the natural vertical thermal gradient present inside the stacking. By comparing with SiC solution growth experiments, convection rolls inside the liquid, which can act as powerful matter transport, were found to form when increasing the liquid Si thickness to few cm [6]. Of course, the thickness values considered in the present work are probably too small for buoyancy-induced convection. However, a strong electromagnetic field, such as the one present inside our RF heated reactor, could activate such a turbulent flow [7,8]. This is because of the high electrical conductivity of liquid Si which makes it easily subjected to induced currents and thus to electromagnetic convection.

In order to confirm the effect of the electromagnetic convection inside the 400 μm thick liquid Si, a sample with that liquid thickness was treated at 1500°C for 30 min using a resistance-heated horizontal furnace. Note that for technical reasons, such apparatus was not adapted to H_2 atmosphere and to temperatures higher than 1500°C so that the treatment was made at this maximum temperature under Ar. The results obtained on this sample are shown in Fig. 3.

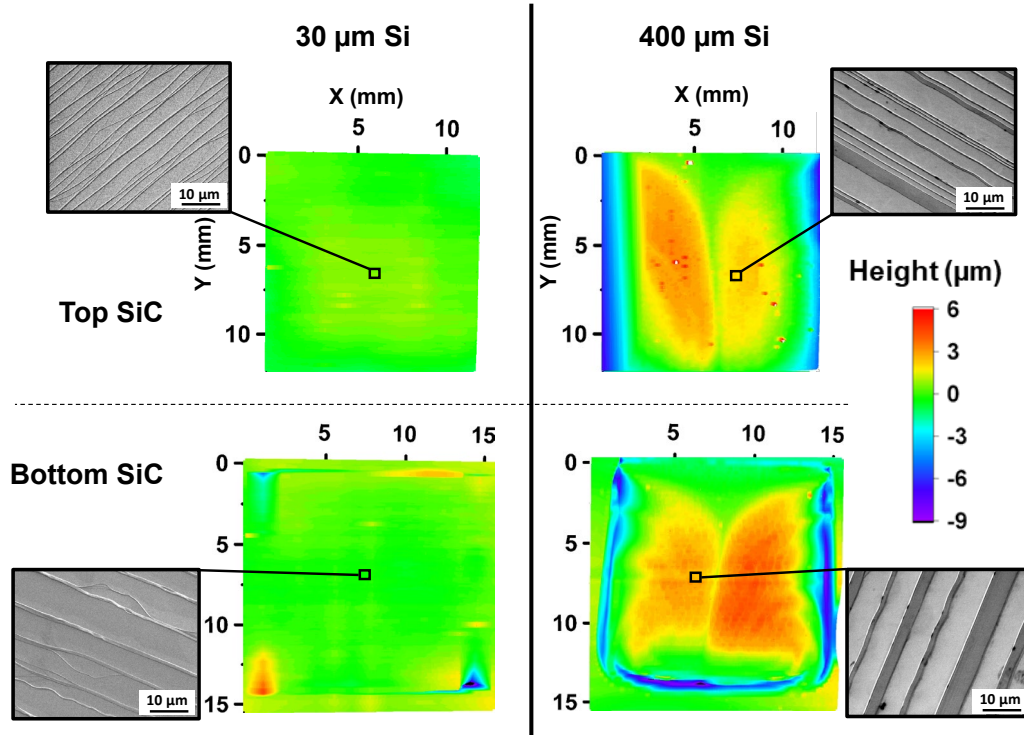


Figure 2. Mechanical profilometry maps obtained on samples treated at 1550°C for 30 min with 30 μm (left) and 400 μm (right) liquid Si thickness. Representative SEM images taken on each wafer are also added.

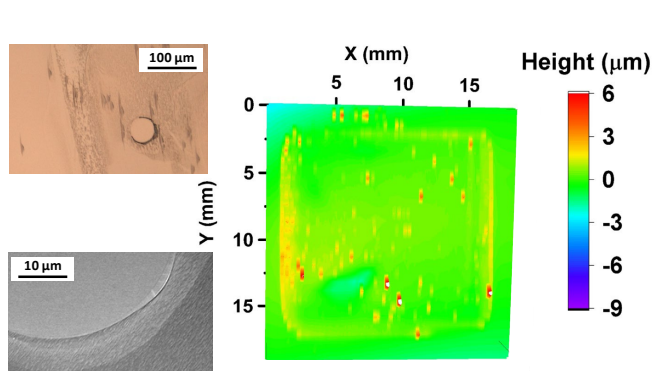


Figure 3. Mechanical profilometry map obtained on the bottom SiC wafer of a sample treated at 1500°C for 30 min with 400 μm thick liquid Si, using a resistance heated furnace. The corresponding surface morphology is shown on the left images taken by optical microscopy (top) and SEM (bottom).

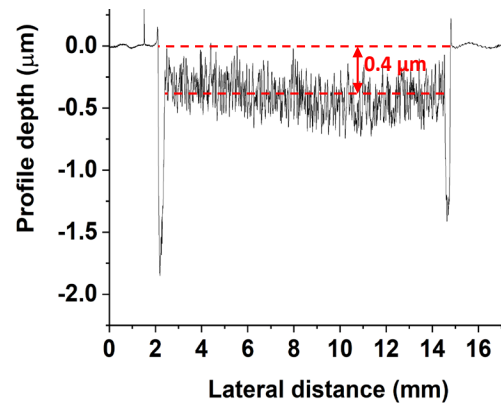


Figure 4. Linear mechanical profile obtained on the bottom wafer of a sample treated 30 min at 1600°C, with 30 μm thick liquid Si.

One can see that the map is much flatter and more homogeneous using the resistance heating than the RF one. The butterfly pattern has disappeared, along with the parallel macrosteps. Some elongated and parallel triangular features are seen which looks like an early stage of macrostep formation. This result confirms our hypothesis of electromagnetic activated convection inside the 400 μm thick liquid. Note the circular print in the optical image of Fig. 3 which is most probably

the result of Ar gas trapping at the SiC-liquid interface, as discussed earlier. This was never seen in the usual H_2 -treated samples.

When increasing the treating temperature to 1600°C with an assembly containing $30\ \mu\text{m}$ thick liquid Si, the surface remains homogeneously flat but now with the appearance of the same edge depressions as seen for $400\ \mu\text{m}$ Si sample in Fig. 2. This is shown in the linear profile of Fig. 4. In addition to these 1.3 to $1.8\ \mu\text{m}$ deep edge depressions, one can see that the average level of the central reconstructed area is $\sim 0.4\ \mu\text{m}$ below the one outside the liquid. Thus, the area in contact with the liquid was not only reconstructed but also etched or dissolved, though in a less pronounced manner than the edges. Assuming a C solubility inside liquid Si in the $0.01\ \text{at}\%$ range at the considered temperatures [9, 10] and $30\ \mu\text{m}$ of liquid Si thickness, this would lead to the dissolution of $\sim 3\ \text{nm}$ of SiC only. This is far from the $0.4\ \mu\text{m}$ found in Fig. 4 which means that the etching in the central area is not just due to saturation of the liquid Si with the C atoms from the SiC wafers. We believe that this dissolution is activated by the vertical thermal gradient which should create a $[C]$ vertical gradient just like in the classical solution growth experiments. By extrapolating to 1h the dissolution value in Fig. 4, one obtains a dissolution rate of $0.8\ \mu\text{m/h}$. We will see later that this value has to be corrected by taking another parameter into account.

Even if H_2 should obviously not interfere with this C transport in the central area, we believe that it can play a role at the edges where these deep depressions are observed. At these places, the liquid Si is in direct contact with H_2 and can thus interact with this gas. Though the formation of SiH_x volatile species cannot be excluded, we believe that reaction between H_2 and the dissolved C atoms could be of more importance. Locally, these dissolved C atoms could form volatile hydrocarbon ($\text{C}_x\text{H}_y(\text{g})$) species, in the same way as reported in [11]. This C atoms removal would thus act as a C pump and locally generate an additional and continuous dissolution of the SiC substrates by the liquid Si.

Analyses of all these results led us to propose two scenarii of mass transport inside the stack depending on the liquid Si thickness. This is summarized in Fig. 5. In the case of $30\ \mu\text{m}$ Si thickness, the vertical thermal gradient imposes the direction of C atoms transport (occurring by diffusion) within the liquid, from the hotter SiC bottom to the colder SiC top (Fig. 5a). As a consequence, the bottom wafer is dissolved while the top wafer receives epitaxial growth. When the liquid Si thickness is increased to $400\ \mu\text{m}$, the RF-induced convection rolls take the lead for matter transport so that the high amount of C atoms released in the liquid at the edges (by the H_2 -induced C pump) could be partially redirected toward the center of the liquid (Fig. 5b). The transport distance and the as-created C supersaturation may be sufficient to generate SiC precipitation and hence epitaxial growth far from the edges. This forced transport of C atoms could lead to precipitation and growth on both SiC wafers. The butterfly pattern observed on the sample with $400\ \mu\text{m}$ Si would then reflect the forced convection scheme that happened inside the thick liquid Si.

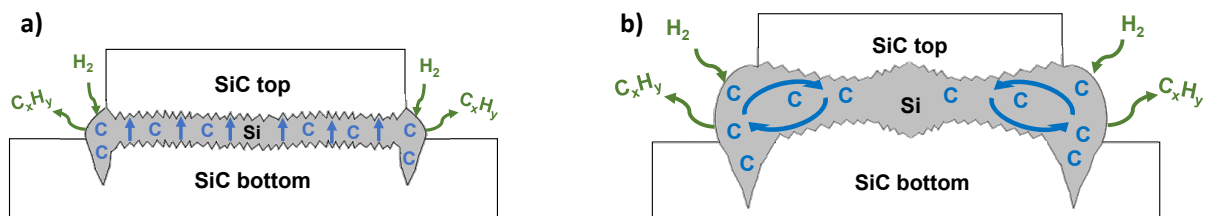


Figure 5. Schematic drawings of the proposed mechanisms occurring for a) $30\ \mu\text{m}$ and b) $400\ \mu\text{m}$ liquid Si thickness within the 4H-SiC sandwich configuration; circle arrows on b) represent the hypothetical direction of convection rolls.

Focusing now on the $30\ \mu\text{m}$ thick Si case, one should consider with care the value of dissolution rate obtained from Fig. 4. Indeed, since SiC is known to be thermally etched by H_2 under moderate rate ($1\text{--}2\ \mu\text{m/h}$ in the temperature range of the present study [12]), the 4H-SiC crystal outside the liquid is most probably etched by H_2 . Consequently, the zero level of the mechanical profilometry, taken outside of the reconstructed area, is not the one of the initial substrate surface before the thermal treatment. In other words, the previously-estimated dissolution rate of $0.8\ \mu\text{m/h}$ at the

center of the sample is probably underestimated and one should add the H₂ etching rate of SiC to this value. This etching rate was determined by treating under H₂ a SiC wafer partially capped with a smaller piece of sapphire wafer. Below this cap, SiC loss by H₂ etching should be drastically reduced as compared to outside the cap. The result obtained from the mechanical profiling on such sample is shown in Fig. 6. This simple capping configuration was effective for protecting the SiC wafer from H₂ etching so that one can estimate this etching rate to $\approx 2.5 \mu\text{m/h}$ outside the cap at 1600°C. If we then correct the dissolution rate of the bottom-SiC wafer by value of H₂ etching rate outside the liquid, we obtain a dissolution rate of $3.3 \mu\text{m/h}$ at 1600°C. Assuming that all the C-dissolved atoms from the bottom wafer are transferred to the top-wafer according to the vertical thermal gradient, this $3.3 \mu\text{m/h}$ should represent the SiC epitaxial growth rate on the top-SiC wafer. Using the same process, the H₂ etching rate at 1550°C was found to be $1.7 \mu\text{m/h}$ and the dissolution rate of the bottom wafer at this temperature was thus of the same value (since the zero level outside the liquid was found at the same altitude below the liquid, see Fig. 2). Of course, one cannot exclude the occurrence of some slow etching of SiC even under the sapphire piece so that the H₂ etching rates and thus the dissolution rates determined here are probably slightly underestimated.

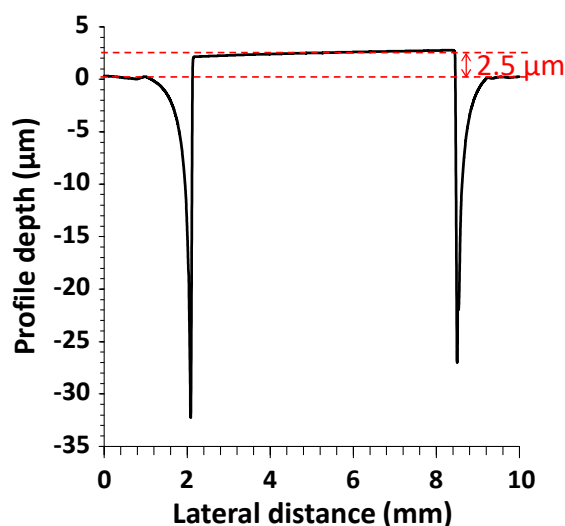


Figure 6. Linear mechanical profile obtained on a SiC wafer capped with a piece of sapphire wafer and treated under H₂ at 1600°C for 1h.

Finally, note in Fig. 6 the deep trenches (down to $32 \mu\text{m}$) on the SiC wafer at the edges of the area occupied by the sapphire piece. We believe that this over-etching could be linked to the lateral H₂ etching of the sapphire which is rather high at such temperature ($\approx 40 \mu\text{m/h}$) and is known to generate O-containing gaseous species such as H₂O [13]. Locally, the high generation of H₂O can increase SiC etching rate and create these trenches.

Conclusion

4H-SiC/Si_(liq)/4H-SiC stacks were treated at 1550-1600°C under H₂ in a RF-heated cold-wall reactor in order to generate macrosteps-structuring of the 4°off SiC(0001) wafers. Using 400 μm thick liquid Si, the observed important matter transport from the edges to the center of the same wafer was attributed to RF-induced convection rolls inside the thick liquid Si. When the liquid thickness was reduced down to 30 μm , the matter transport followed this time the vertical thermal gradient like in the case of liquid phase epitaxy. The dissolution rate of the bottom (hotter) wafer was found to increase from $1.7 \mu\text{m/h}$ at 1550°C to $3.3 \mu\text{m/h}$ at 1600°C. The use of H₂ gas was found essential to the system since it does not generate gas trapping (unlike Ar) and it participates to the creation of the vertical thermal gradient.

Acknowledgement

This work has been financially supported by French ANR in the framework of the 19-CE24-0007 "Risemos" project.

References

- [1] J. Woerle, B. C. Johnson, C. Bongiorno, K. Yamasue, G. Ferro, D. Dutta, T. A. Jung, H. Sigg, Y. Cho, U. Grossner, and M. Camarda, *Phys. Rev. Mater.*, 3, (2019) 84602
- [2] I. D. P. Fiorenza, F. Iucolano, G. Nicotra, C. Bongiorno, F. A. L. Magna, F. Giannazzo, M. Saggio, C. Spinella, F. Roccaforte, *Nanotechnology*, 29, (2018) p. 39
- [3] M. Camarda, J. Woerle, V. Souliere, G. Ferro, H. Sigg, U. Grossner, and J. Gobrecht, *Mater. Sci. Forum*, 897, (2017) p. 107
- [4] Y. Jousseau, F. Cauwet, G. Ferro, *Mater. Sci. Forum*, 1062 (2022) p. 8
- [5] X. Xing, T. Yoshikawa, O. Budenkova, D. Chaussende, *J. Mater. Sci.* 57 (2) (2022) p. 972
- [6] F. Mercier, J. M. Dedulle, D. Chaussende, M. Pons, *J. Cryst. Growth*, 312, 2, (2010) p. 155
- [7] U. Burr, U. Müller, *J. Fluid Mech.*, 453, (2002) p. 345
- [8] Y. Tasaka, T. Yanagisawa, K. Fujita, T. Miyagoshi, A. Sakuraba, *J. Fluid Mech.*, 911 (2021) p.1
- [9] R. I. Scace, G. A. Slack, *J. Chem. Phys.*, 30, (1959), p. 1551
- [10] K. Yanaba, M. Akasaka, M. Takeuchi, M. Watanabe, T. Narushima, Y. Iguchi, *Materials Transactions*, 38, 11 (1997) p. 990.
- [11] K. Alassaad, V. Soulière, F. Cauwet, D. Carole, G. Ferro, *Mater. Sci. Forum*, 821–823, (2015), p. 121
- [12] C. Hallin, F. Owman, P. Martensson, A. Ellison, A. Konstantinov, O. Kordina, E. Janzén, *J. Cryst. Growth*, 181, (1997), p. 241
- [13] L.A. Marasina, V. V. Malinovsky, I. G. Pichugin, P. Prentky, *Cryst. Res. & Technol.* 17 (3) (1982) p.365